DTIC FILE COPY

Naval Research Laboratory

Washington, DC 20375-5000

NRL Memorandum Report 6674

AD-A223 929

Soft X-ray Emission Spectra from Laser-Irradiated High-Z Targets

G. MEHLMAN,* P. G. BURKHALTER, D. A. NEWMAN* AND B. H. RIPIN

Dynamics of Solids Branch
Condensed Matter and Radiation Science Division

**Sachs/Freeman Associates, Inc.*
Landover, Maryland 20785

DTIC
ELECTE
JUL 16 1990
S D
D

June 29, 1990

Approved for public release; distribution unlimited.

90 07 16 024

REPORT DOCUMENTATION PAGE

Form Approved
OMB No. 0704-0188

Public reporting burden for this collection of information is estimated to average 1 hour per response, including the time for reviewing instructions, searching existing data sources, gathering and maintaining the data needed, and completing and reviewing the collection of information. Send comments regarding this burden estimate or any other aspect of this collection of information, including suggestions for reducing this burden, to Washington Headquarters Services, Directorate for information Operations and Reports, 1215 Jefferson Davis Highway, Suite 1204, Arlington, VA 22202-4302, and to the Office of Management and Budget, Paperwork Reduction Project (0704-0188), Washington, DC 20503.

1. AGENCY USE ONLY *(Leave blank)*	2. REPORT DATE	3. REPORT TYPE AND DATES COVERED
	1990 June 29	Memorandum

4. TITLE AND SUBTITLE
Soft X-ray Emission Spectra from Laser-Irradiated High-Z Targets

5. FUNDING NUMBERS

6. AUTHOR(S)
Mehlman,* G., Burkhalter, P.G., Newman,* D.A., and Ripin, B.H.

7. PERFORMING ORGANIZATION NAME(S) AND ADDRESS(ES)
Naval Research Laboratory
4555 Overlook Ave., S.W.
Washington, DC 20375-5000

8. PERFORMING ORGANIZATION REPORT NUMBER
NRL Memorandum Report
Report 6674

9. SPONSORING/MONITORING AGENCY NAME(S) AND ADDRESS(ES)
Defense Nuclear Agency
Washington, DC 20301-1900

10. SPONSORING/MONITORING AGENCY REPORT NUMBER

11. SUPPLEMENTARY NOTES
*Sachs/Freeman Associates, Inc.

12a. DISTRIBUTION/AVAILABILITY STATEMENT
Approved for public release; distribution unlimited.

12b. DISTRIBUTION CODE

13. ABSTRACT *(Maximum 200 words)*

X-ray data were acquired from mass-limited targets with the Pharos III laser system. Targets, mounted at the tip of thin glass stalks, were microscopic pieces of single or multiple high-Z element composition. The laser irradiance was 4×10^{14} W/cm^2 with about 300J of focused 1.05 μm wavelength laser beam.

A convex KAP crystal spectrograph was used for its capability to collect high resolution spectra in the 4-20 Å soft x-ray region. The recorded spectral film densities were microdensitometered and converted by computer-processing to absolute continuum and emission line intensities. The spectral features were identified with the aid of ab-initio atomic structure calculations. The continuum background was evaluated as a source of pseudo-continua for absorption studies of soft x-rays.

14. SUBJECT TERMS	15. NUMBER OF PAGES
X-ray spectroscopy Laser-heated plasmas Continuum emission	27
	16. PRICE CODE

17. SECURITY CLASSIFICATION OF REPORT	18. SECURITY CLASSIFICATION OF THIS PAGE	19. SECURITY CLASSIFICATION OF ABSTRACT	20. LIMITATION OF ABSTRACT
UNCLASSIFIED	UNCLASSIFIED	UNCLASSIFIED	UNLIMITED

CONTENTS

DTIC COPY INSPECTED 8

Accession For
NTIS CRA&I
DTIC TAB
Unannounced
Justification
By
Distribution /
Availability Codes
Dist | Avail and/or Special
A-1

SOFT X-RAY EMISSION SPECTRA FROM LASER-IRRADIATED HIGH-Z TARGETS

INTRODUCTION

There is strong interest in the development of sources of x-ray emission of continuous or quasi-continuous spectral character for quantitative absorption spectroscopy of micron-size plasma regions. Pulsed sources of hot and dense plasma can deliver intense x-ray pulses. Two basic types of pulsed plasmas have been investigated, namely the pulsed power systems such as Z-pinch generators[1] or plasma focus devices and focused-laser produced plasmas. Because of the possibility of focusing laser beams onto submillimeter areas of the irradiated targets, the generated plasmas represent the closest approach to well-defined, reproducible, small-size sources of x-rays suitable for probing small, reasonably uniform regions of plasma. We have used this technique to measure continuous or semi-continuous emission in the soft x-ray range 4-16 Å.

Studies of laser-produced continua have been carried out in the 40-2000 Å range for the elements samarium to ytterbium[2] and more recently in the x-ray region[3] for a wide range of elements. However, in numerous dense plasma emission studies, especially from intermediate-Z elements ($Z \geq 42$), the work focuses on identification and classification of the observed transitions or transition arrays[4,5,6]. High-Z element spectra from tungsten, gold and lead were also observed at wavelengths above 20 Å by Finkenthal et al.[7] using the TEXT plasma.

When the goal is the generation of continuous radiation from laser-heated plasmas the target selection criteria become choosing elements of medium- or high-Z for their capability of supplying ion populations from a large number of stages corresponding to M- or N-shell electronic structure $3d^n$ or $4f^{n'}$ respectively (n number of 3d electrons, n' number of 4f electrons in ground state).

Manuscript approved May 7, 1990.

In the present experiment, soft x-ray emission spectra were collected from two groups of targets containing, in the first one, medium-Z elements Te, Ba or La, in the second one, high-Z elements gold, bismuth, and uranium. The selected intermediate-Z elements (Te, Ba and La) were contained in compounds. The Ba compound namely $BaBi_{0.4}Pb_{0.6}O_3$, was especially studied to observe at once emission from the combined high-Z elements Bi and Pb and from the medium-Z element Ba.

In the 10-16 Å range the observed spectra from the medium-Z ion plasmas exhibit broad band or pseudo-continuum structure. We attributed these observed successive bands of unresolved transitions to $3d^n$ - $3d^{n-1}4f$ transition arrays from the element (Te, Ba or La) successive ions with $3d^n$ outer electron structure in ground state ($1 \leq n \leq 10$). The array identification was made with the aid of atomic structure computations of the excited levels. Each array average spectral extent is of the order of 0.3 Å and occurs at higher energies with decreasing n, by amounts reflecting roughly the ionization potential difference between two successive ions. These bands would be suitable for the observation of K- or L-shell absorption edges from thin foils.

Such complex spectra produced by multi-ionization stages of medium-Z species (often labelled "quasicontinuum"[8] or unresolved transition arrays "UTA"[9]) have been observed in the soft x-ray range and identified for a number of intermediate-Z elements such as Sm, Gd, Dy[4], Nb[10], Sn[11], La[12], and Tm, Yb, Hf, Ta, W, Re, Pt[5]. The 3d-4f transitions of gold have also been extensively observed in a higher-energy spectral range[13]. The higher-Z material ($Z>78$) targets should supply ions with $4f^{n'}$ ground state configuration structure ($1 \leq n' \leq 14$), therefore poteneially more contributing ionization stages than the $3d^n$ shell and much more complex transition arrays.

We observed in the recorded spectral range (4 to 16 Å) fairly continuous

radiation from the high-Z elements studied with intensity increasing with wavelength. We correlated this variation with free-free and free-bound radiation from the much denser plasma. The broad emission structure observed in these spectra superimposed on the continuum has been associated with N-shell transition arrays using atomic structure calculations to predict their energy location.

EXPERIMENTAL

Microtargets of high-Z elements or compounds were irradiated with the Naval Research Laboratory Pharos III laser system. The Nd:glass laser beam delivers 1.054 μm-wavelength photons with total energy between 285 and 300 joules and 4.5 ns duration. The beam was focused perpendicular to the target (or target holder) with a spherical lens system giving a 140 μm-diameter focal spot.

The compound targets were microfragments of average dimension of the order of 150 μm broken from larger chunks of specially prepared compounds ; some single-element targets, such as bismuth, were high purity microspheres supplied by the manufacturer. They were glued on glass stalks held perpendicular to the incident beam. Thin gold wires 50 μm-diameter and small-area gold foils or uranium ribbons were also used. The gold foils (a few μm-thick) or uranium ribbons (50 μm-thick) were stretched in an appropriately shaped holder. The gold foil was burnt through by the laser beam while the thicker uranium ribbon behaved as a slab.

The emission from the plasma created by laser irradiation of the microtarget was observed with an x-ray spectrograph equipped with a convex-potassium acid phtalate (KAP) crystal (3.175 cm radius) and a thin beryllium window opaque to visible light. The calculated resolution for the reflection from KAP (001) planes is of the order of 4 mÅ around 8 Å[14]; however the experimental resolution was poorer (~35 mÅ) because of source size broadening. The microtargets were photographed so that their size could be determined. A microscope photograph of one of them is shown in Fig.1. The target dimension perpendicular to the laser beam defines an upper limit for the resolution since we have not measured, in this experiment, the x-ray emitting region actual size.

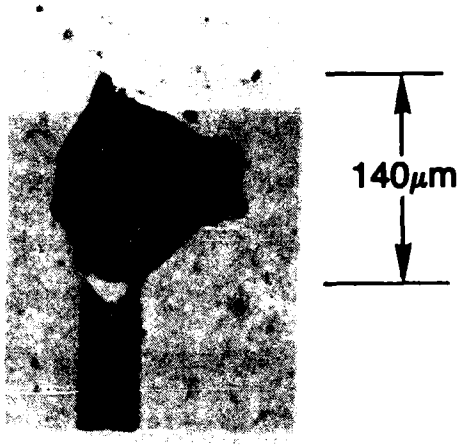

Fig. 1 — Microtarget ($BaBi_{0.4}Pb_{0.6}O_3$) mounted on a glass stalk

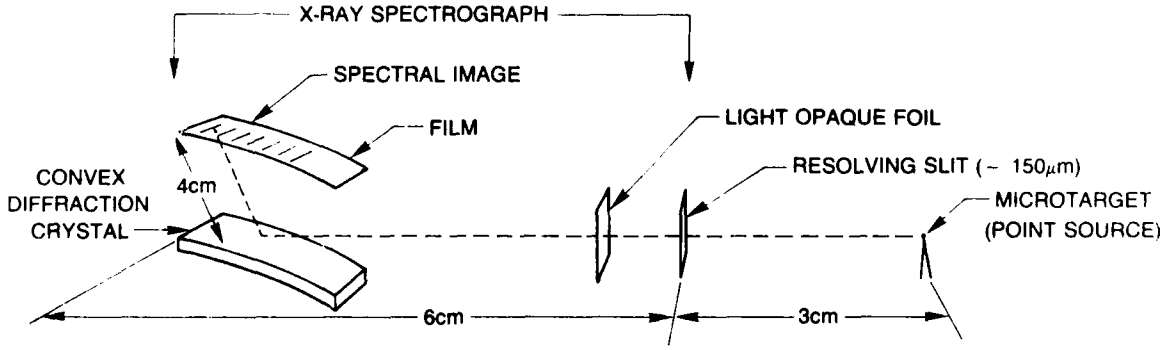

Fig. 2 — Experimental arrangement with typical dimensions

The time-integrated spectrum recorded for each laser irradiation on a cylindrically curved DEF film, covered the spectral range 4.5-20 Å; however, we limited the upper wavelength value to 16 Å for accurate absolute intensity determination since the intensity conversion accuracy deteriorates with increasing wavelength because of the decreasing transmission of the 7.5 μm-thick Be foil (18% at 16 Å as opposed to about 80% at 8 Å). A schematic of the spectrograph illumination is shown in Fig.2. To protect the spectrograph window from debris a slit about ~150 μm-wide was located in front of it at a distance of 6.5 cm from the crystal apex and perpendicular to the crystal axis (Fig.2).

The recorded spectrograms were scanned with a densitometer using a 400 μm slit height that is shorter than the ~600 μm with the above geometry, projection of a point source onto the film plane. The film densities were computer-processed to obtain true intensities in eV/sr-Å using published DEF film calibration[15], calculated integral reflection coefficients for the curved diffraction crystal[16], published data on beryllium absorption coefficients, and modeling for the source-crystal-film geometry and curved-crystal optics[17].

Calculations were performed for the $3d^n \rightarrow 3d^{n-1}4f$ (M-shell) transition array energies using R. Cowan's atomic structure code written at L.A.N.L.[18] for the ab initio atomic level computations. The same calculations for ions with $4d^{10}4f^{n'}$ ground level (N-shell transitions) are exceedingly more complex than for the ions with $3d^n$ ground level. In order to identify both the most probable contributing ionic stages and the 4ℓ-$5\ell'$ transition arrays responsible for the observed intensity "bumps" in gold, bismuth and uranium spectra, we computed ab initio individual level calculations considering solely transitions from ions with ground state $4d^{10}4f^{n'}$ and excited states either $4d^9 4f^{n'} 5\ell$ (ℓ=f,p) or $4d^{10}4f^{n'-1}5\ell$ (ℓ=d,g) namely those transitions with the largest transition probability.

For further allievating the computations in the case of the uranium spectra, we defined the predicted transition energy range by computing the above excited levels only for n'-1 and n'-14. It should also be noted that we limited the computations of the ion discrete radiation to transitions with $\Delta n=1$ with the exception of barium M-shell transitions 3d-5f and 6f in the $3d^n$ ion sequence.

RESULTS

With the geometry described in the preceeding section, the one-dimensional spatial resolution of the plasma is of the order of 200 μm which in all cases is larger than the intense x-ray emission plasma volume. Thus, the spectral image was merely the slit projection onto the film plane. With a typical microfragment of about 150 μm largest dimension, the spectral resolution was better than about 35 mÅ over the whole range 7-16 Å.

When larger-size plasmas were generated from foil targets, a narrow 50 μm-slit was used to compensate for the more intense radiation and to improve to some extent the reduced resolution. Under these conditions, with the gold foil target, we obtained a spectral image with uniform density perpendicudar to the dispersion direction that is along the extent of the illumination from a point source. On the contrary, with the thicker uranium target, a region about 100 μm in length with larger optical density was noticeable along the image extent.

The microfragments, which were favored as the closest approach to a point x-ray emission source, introduced impurity components in the plasma such as : sodium, magnesium, silicon and sulfur from the glass stalk and glue. These low-Z elements supply hydrogen- and helium-like ions with their intense 1s-2p transitions over the recorded wavelength range. These lines provided calibration wavelengths over the continuum emission so that the wavelength accuracy is of the order of ± 0.005 Å for isolated lines. Figure 3 shows an intensity trace in the range 4.5-11.5 Å with the calibration lines indicated. Generally, weak sodium and silicon lines were found on all the medium-Z element spectra but for the self-supported large-area targets of pure gold or uranium no impurity line

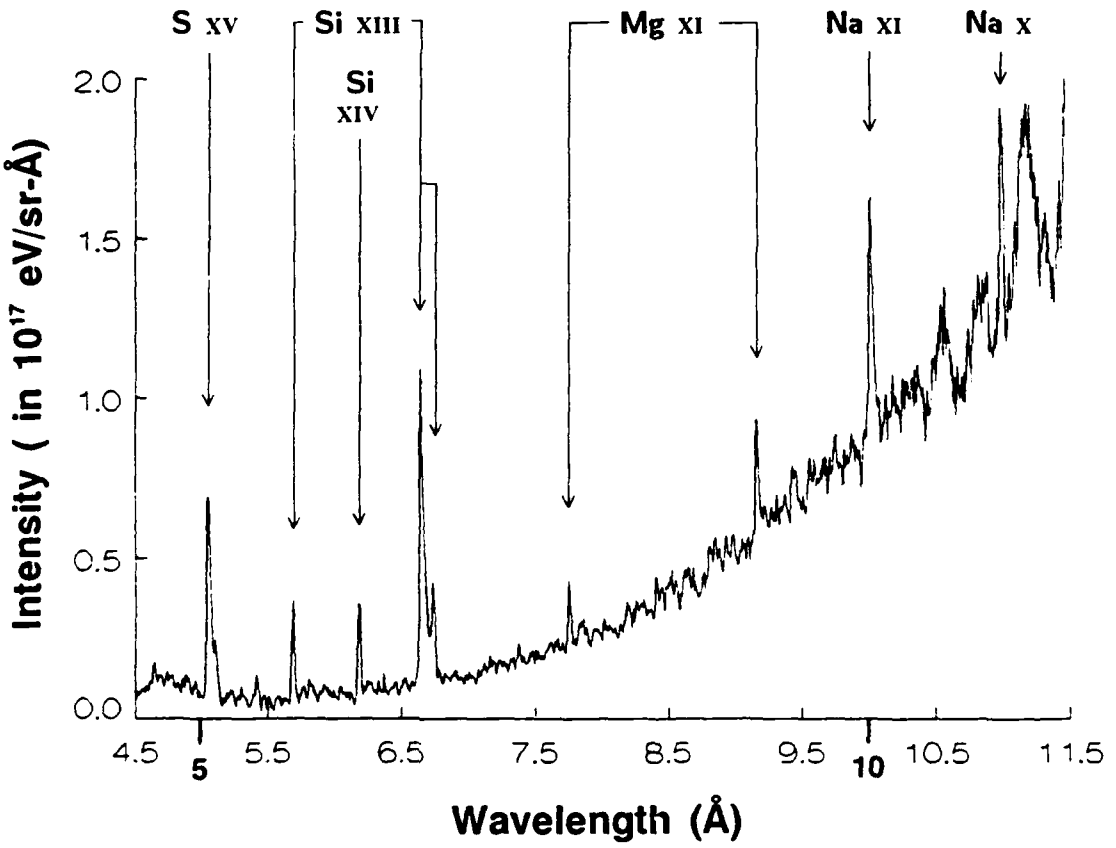

Fig. 3 — Spectral intensity trace from a $BaBi_{0.4}Pb_{0.6}O_3$ microfragment with impurity lines used for wavelength calibration

appeared in the spectra and we had to superimpose the spectral image on a spectrum with impurity lines for a rough wavelength calibration of the gold or uranium continuum. The wavelength accuracy on the gold and uranium traces (see below) is therefore only of the order of ± 0.1 Å.

We first collected spectra from a variety of compounds containing intermediate-Z elements ($40 < Z < 70$) suitable for M-shell emission in the recorded spectral range. We shall discuss in sub-section A) the tellurium, barium and lanthanum emission obtained from targets made of the compounds: $TeAg_2$, $BaBi_{0.4}Pb_{0.6}O_3$ and $LaCu_{0.5}Cr_{0.5}O_3$, respectively.

Second, we recorded spectra from irradiated targets made of gold, pure bismuth, bismuth compounds and uranium with respective atomic number Z=79, 83 and 92 with the goal of observing N-shell emission. A more detailed discussion of the N-shell emisson from U, Bi and Au appears in the sub-section B) below.

All spectra exhibit intense continuum emission onto which, in the case of the intermediate-Z elements, spectral bands corresponding to the M-shell unresolved transition arrays are superimposed; these will be identified in the sub-section below for Te, Ba and La. The continuum level is much higher and more uniform in the three high-Z element spectra and we observed only intensity increases or shoulders when proceeding from short to long wavelengths (which we shall call "bumps"); this is particularly clear in the uranium emission. The predicted arrays from N-shell emission were calculated and correlated with these observed bumps. The fairly distinct spectral character between the M-shell and the N-shell emissions suggests that free-free or free-bound radiation predominates in the second case. For M-shell emission, unresolved transition arrays dominate the spectra.

In the high-Z element spectra, linear fits to the continuum intensity slope

(on plots of the intensity logarithm versus photon energy) lead to an electron temperature estimate in the region of the plasma emitting primarily continuum. The temperature values derived by this method are around 190-210 eV for an uranium plasma while the bismuth intensity slope corresponds to about 260 eV and gold to 230 eV.

A) M-shell spectrum from Te, Ba and La

The emitted spectrum from laser irradiation of the compound microfragments containing tellurium, barium or lanthanum was recorded for each shot. Spectral traces representative of the reduced absolute intensity versus wavelength are shown in Fig.4 (a,b and c) for three spectra corresponding to each compound. In each trace a series of emission bands characteristizes the spectrum; the separation of the band peak emissions is of the order of 0.3Å, in some relation with the ionization potential increasing value with decreasing number of outer electrons in an ion sequence. We note the shift of the band sequence towards high energy with increasing Z, from tellurium to lanthanum, reflecting the higher ionization degree of the contributing ions. Consequently the wavelength range shown in the figure changes from 12.5 to 16 Å for tellurium to 10 to 14 Å for barium and 9.5 to 13.5 Å for lanthanum.

The observed band series may be associated with the series of well-defined $(n\ell)^x \rightarrow (n\ell)^{x-1}\, n'\ell'$ unresolved transition arrays from the ion sequence with varying number of electrons in their ground state $(n\ell)$. The particular transition arrays that occur over the observed energy range can only be 3d-4ℓ (ℓ=p,f). The 3d-4p arrays which lie at longer wavelengths (calculated to be between 13.9 and 21.4 Å for Te, between 11.3 and 16.5 Å for Ba and between 10.8 and 15.5 Å for La) are much weaker than the 3d-4f and were not identified. In

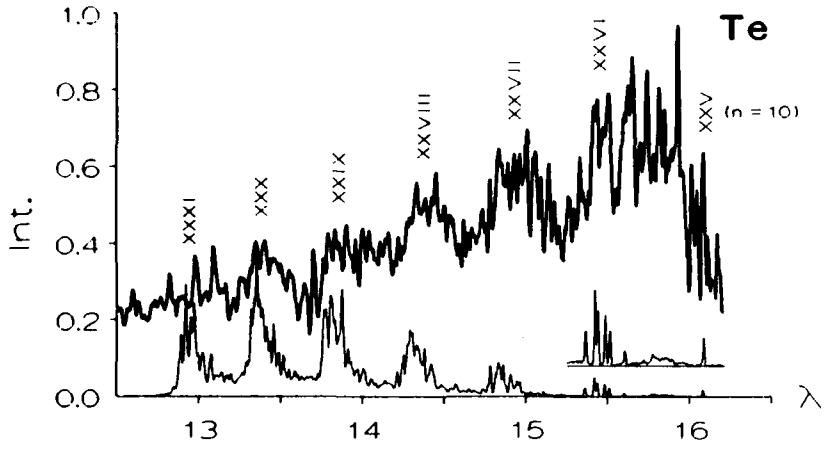

a)

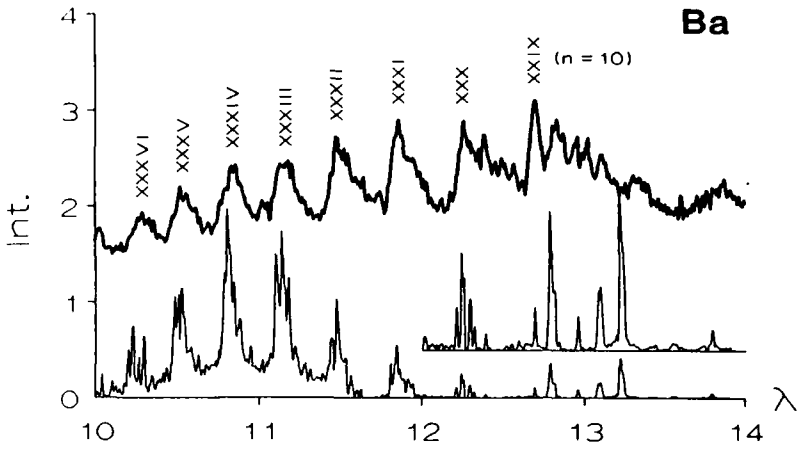

b)

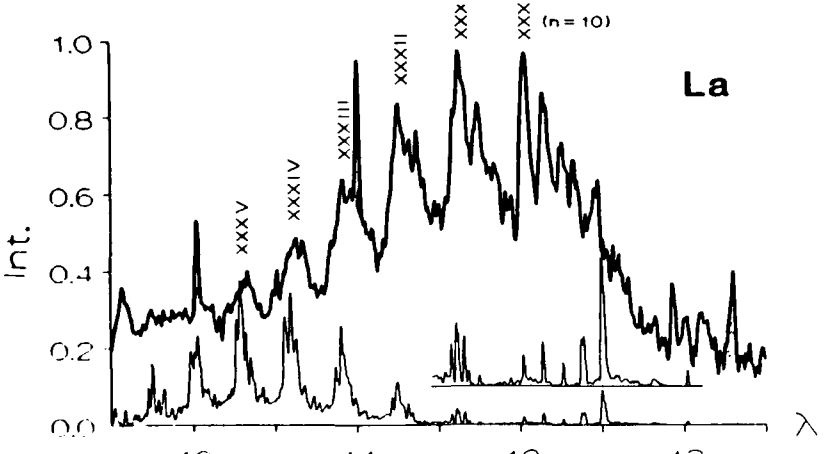

c)

Fig. 4 — The $3d^n \rightarrow 3d^{n-1}4f$ transition sequence (starting at n=10) and some $3d'^{10}(4\ell) \rightarrow 3d'^{9}(4\ell)4f$ transitions for: a) Te, b) Ba, c) La.

The upper traces (bold) are the experimental intensity spectra with units in 10^{17} eV/sr-Å and wavelength scale in Å for: a) $TeAg_2$, b) $BaBi_{0.4}Pb_{0.6}O_3$, c) $LaCu_{0.5}Cr_{0.5}O_3$ targets. Shaded lines in the la trace are superimposed impurity radiation from sodium ls-2p transitions (NA XI, Na X ions) and silicon (Si XIII ls-2p) in second order. The lower traces are the calculated gA values for the various ion stages indicated above each transition array.

all cases the observed band system was straightforwardly associated (from ab initio calculations) with the $3d^n \rightarrow 3d^{n-1}4f$ transition arrays in the corresponding ion sequence with $3d^n$ ($1 \leq n \leq 10$) outer structure. The sequence is almost complete for barium with $2 \leq n \leq 10$.

We computed the spectral energy and the gA values (g statistical weight, A radiative transition probability) for the $3d^n \rightarrow 3d^{n-1}4f$ transition arrays in these elements. Below each experimental trace in Fig.4 is a plot constructed with gaussian line profiles with constant width 0.01 Å and peak equal to the transition calculated gA value at the calculated energy location (converted to Å). On the long wavelength side of the scans (Fig.4b and c), corresponding to ions with full $3d^{10}$ subshell, we observed contribution from the "satellite" transitions 3d → 4f from lower ionization stages. For instance the 3d-4f transitions from ions with ground configuration: $3d^{10}4s$, $3d^{10}4s^2$, $3d^{10}4s^24p$, $3d^{10}4s^24p^2$ and $3d^{10}4s^24p^6$ (the 3d subshell being labelled $3d'^{10}$ on the figure) have been calculated and their gA values are also plotted on the lower trace for identification purposes only. On the long wavelength side of the plots the gA values appear also on an enlarged scale. The agreement between observed spectrum and predicted transitions is quite good especially for barium (Fig.4b).

We also calculated the higher energy transitions for barium ions with $3d^{n-1}5f$ and 6f excited states (ion sequence with $3d^n$ ground state). These transitions are identified in Fig.5 in the 5-11 Å range. The intensity trace was obtained from the same barium compound ($BaBi_{0.4}Pb_{0.6}O_3$) as in Fig.4b and on the long wavelength side, the same Ba bands are recognizable. The calculated gA values for these transitions are plotted below the experimental spectrum in Fig.5. Agreement with the observed weak structure is reasonable.

The sucessive ionization degrees of the radiating ions are indicated

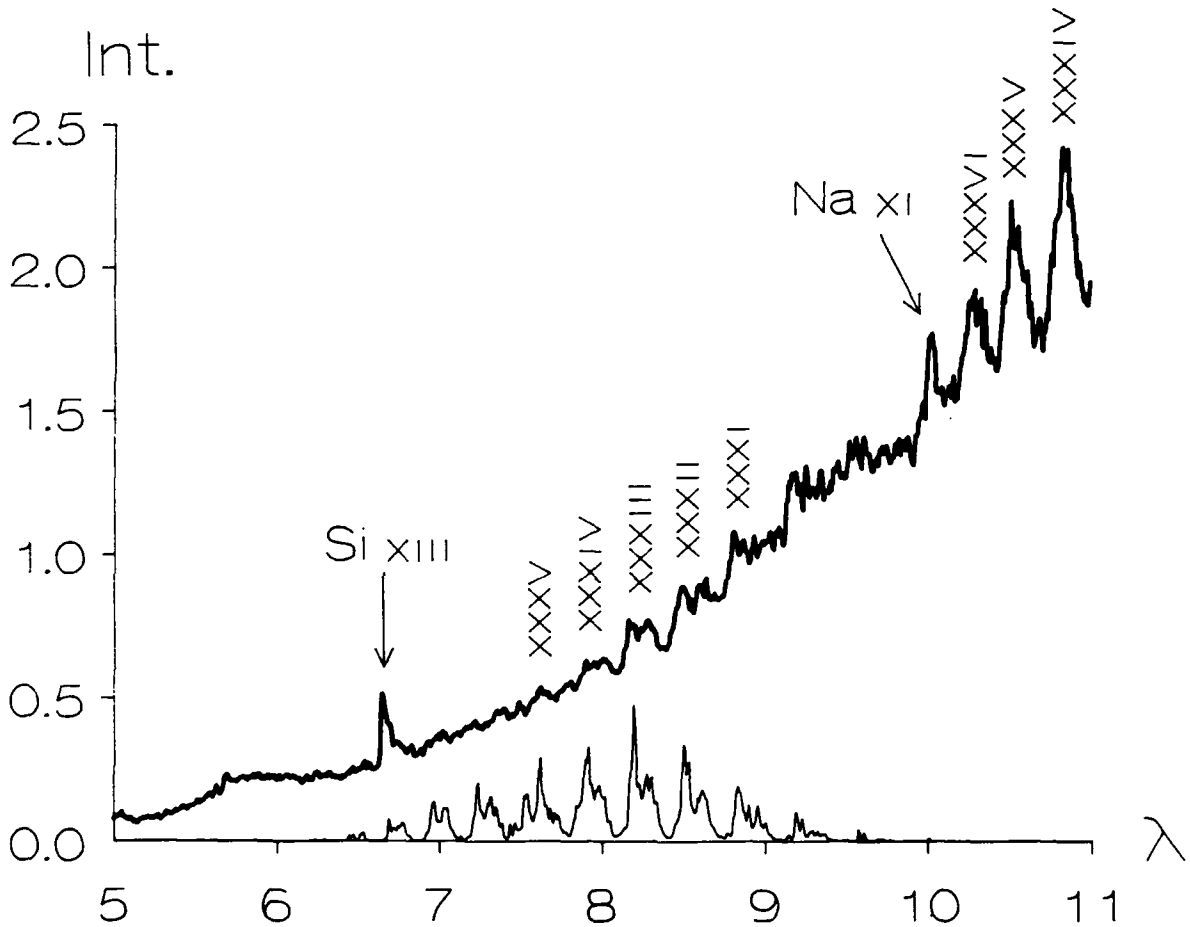

Fig. 5 — Experimental intensity trace from a laser-irradiated $BaBi_{0.4}Pb_{0.6}O_3$ compound (intensity in 10^{17} eV/sr − Å and wavelength in Å). The lower trace is a plot of the calculated gA values for the Ba ion transition sequence with $3d^{n-1}5f$ and 6f excited states.

in Fig.4 a,b,c and in Fig.5 above the unresolved arrays. On the lanthanum spectrum the impurity lines are shaded because of their large intensity in that particular shot. For all three elements, the large intensities observed for the transitions from ions with $3d^{10}$, $3d^{9}$, $3d^{8}$ ground state, compared to the predicted relative gA values for the whole sequence, establish these ion dominant populations in the plasma. Ionization degrees from XXV (Te) to XXXII (La) for these elements with atomic number in the range 52-57 are therefore representative of the plasma temperature reached with the laser power available.

B) N - shell transitions in heavier ions

Figure 6 shows spectral traces obtained in the 10-16 Å range from irradiation of a gold foil, a pure bismuth microsphere and an uranium ribbon.

In this spectral range one expects to recognize predicted N-shell transitions involving ions with primarily $4p^{m}$ and $4d^{n}$ ground level for gold and $4d^{n}$ and $4f^{n'}$ ground level for bismuth and uranium of higher atomic number. In the gold spectrum the 4d-5f group with the largest gA values is expected to dominate the spectrum. In the other elements the 4f-5g transitions contribute the most.

a) gold spectrum

At wavelengths longer than 7Å gold should radiate primarily $4p \rightarrow 5\ell$ (ℓ=s,d) and 4d-5f transitions from ions of lower ionization degree than Au L ($3d^{10}4s^{2}$ ground level). The 4d-5p transitions lie above 17 Å.

We calculated the 4p-5ℓ and 4d-5f energy positions and gA values for gold ions Au XXXIV to XLIX that is through a sequence from $4p^{6}4d^{10}$ to $4p^{1}$ ground level. Also, the $4p^{6}4d^{n} \rightarrow 4p^{5}4d^{n}5\ell$ ($1 \leq n \leq 10$) so-called "satellite" transitions were computed. The calculated gA values for all these transitions were plotted in the lower trace of Fig.6a as gaussian line profiles with constant width 0.01 Å.

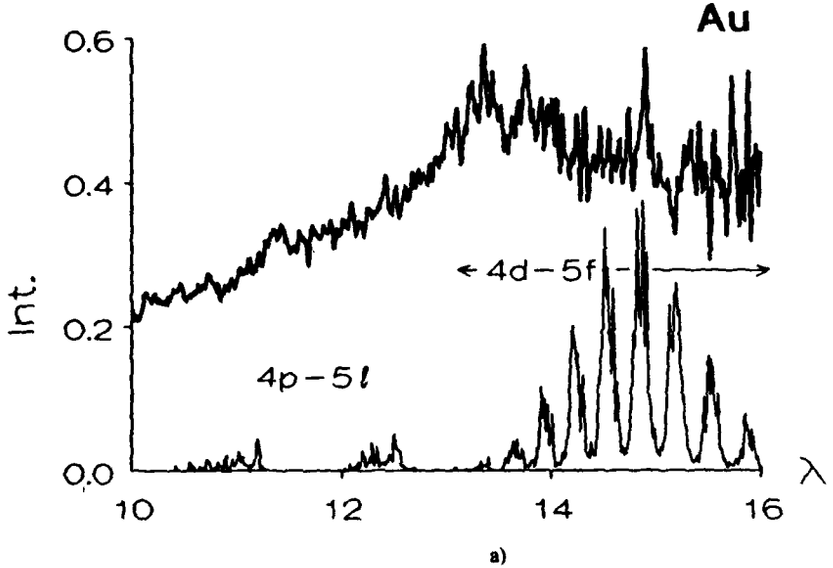

a)

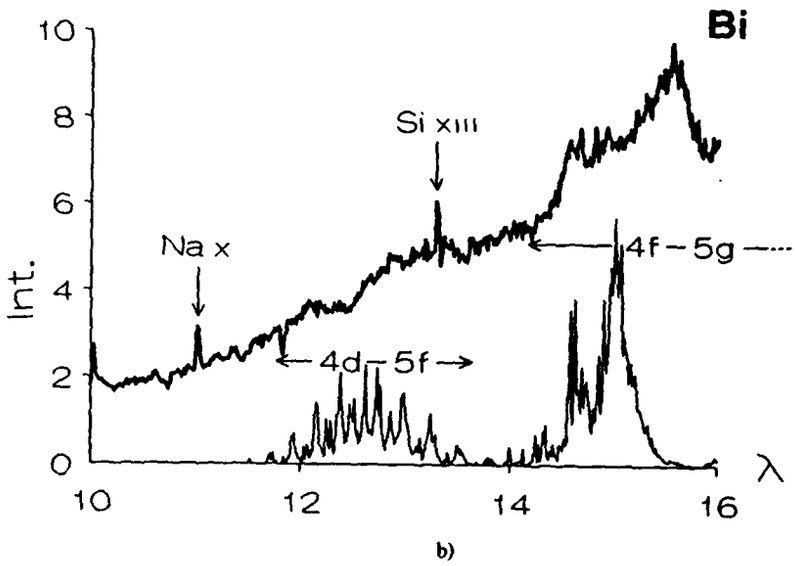

b)

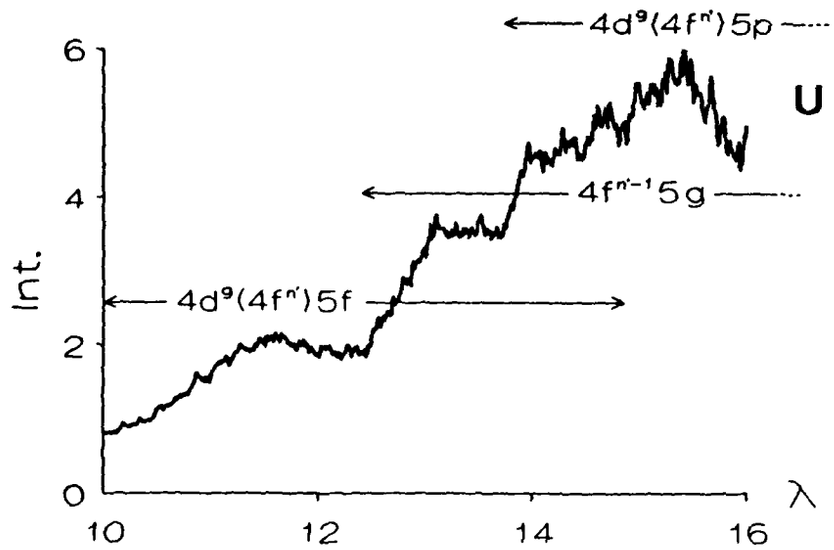

c)

Fig. 6 — Experimental intensity traces from laser-irradiated a) gold, b) bismuth, c) uranium targets with intensity units in 10^{17} eV/sr – Å and wavelength scale in Å. The lower traces are plots of the calculated gA values for: a) the Au $4d^n \rightarrow 4d^{n-1}5f$ and $4p^6 4d^n \rightarrow 4p^5 5l$ (l = s,d) sequences, b) the Bi $4 \rightarrow 5$ transition sequences as described in text. In c) the upper states of uranium ion transitions for ions with $4d^{10}4f^{n'}$ ground state are indicated on horizontal lines (uranium ion sequence U XXXIII to U XLVI). The line extent represents the sequence wavelength range.

We observe that the 4d-5f transition groups from Au XXXIV to XLIII (with much larger gA values) at predicted wavelengths betweeen 13.5 and 16 Å agree reasonably with the intensity increase above 13 Å. The relatively much weaker groups of $4p^m$-$4p^{m-1}5\ell$ transitions were calculated to lie between 10 and 11 Å. The equally weak satellite transitions were found to extend between 10.8 Å and 18.2 Å (with comparable radiative probability from all ionization stages). The maximum emission may be interpreted as evidence for large ion populations of Au XLIII to roughly Au XL.

In Fig.7 is shown the gold spectrum in the 4-11 Å region. The previously identified M-shell transitions (3d-4f, 4p and 3p-4d)[13] are indicated on the high energy side (4 to 6 Å region). The M-shell emission indicates the existence in the plasmas from higher Z elements of much more highly ionized ions such as Au LI - LIV.

b) bismuth spectrum

In the bismuth spectrum (Fig.6b) we observe a smooth continuum emission of increasing intensity with wavelength with two pronounced steps: the first one around 14.5 Å followed by another bump around 15.25 Å.

We calculated the 4d-5ℓ (ℓ = p,f) and 4f-5g transition energy positions and gA values for bismuth ions Bi XXXVIII to XLVII with $4d^n$ outer structure and for ions BiXXXVII to XXXIV with $4f^{n'}$($1 \leq n' \leq 4$) ground level. The 4p-5d satellite transitions in the ions with $4p^6 4d^n$ ground level were also calculated as well as the 4d-5ℓ (ℓ = p,f) satellites in the ions with $4f^{n'}$ outer shell ($14 \geq n' \geq 1$) namely Bi XXXVII to Bi XXIV. The lower trace in Fig.6b is a plot of these calculated gA values for the $4d^n \rightarrow 5f$ ($1 \leq n \leq 10$), the much weaker $4d^n \rightarrow 5p$ and the $4f^{n'} \rightarrow 5g$ ($1 \leq n' \leq 4$) transitions.

The 4d-5f transition sequence lies between 11.65 and 14 Å and therefore

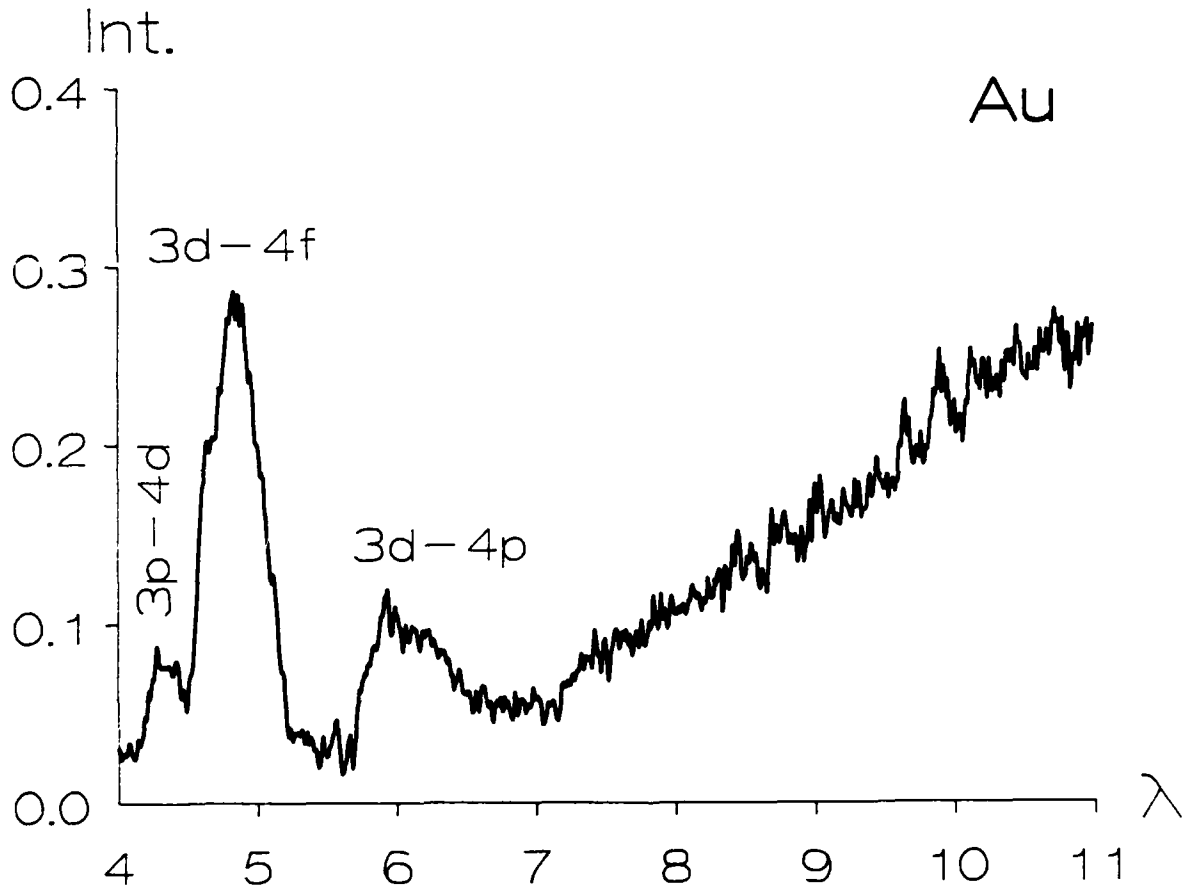

Fig. 7 — Spectrum from a laser-irradiated gold foil in the 4-11 Å range with intensity units in 10^{17} eV/sr−Å and wavelength in Å. The 3 → 4 transition arrays are indicated.

may be correlated with the smooth emission between 12 and 14 Å; the much weaker 4d-5p sequence lies between 15 Å (Bi XLVII) and 19 Å (Bi XXXVIII). The 4p-5d satellite transitions are found between 10 and 12 Å, the 4d-5p satellites occur at longer wavelengths not recorded with the instrumentation and the 4d-5f satellites should contribute to the emission above 14 Å. The 4f - 5g transitions (calculated for n'=1 to 4 only) agree reasonably well with the observed intensity increase around 14.5 Å. The smooth slope from 10 to 13 Å may also be correlated to a number of 4p-5ℓ (ℓ=s,d) multiplets from the same ionization stages such as: $4p^6 4d^n \rightarrow 4p^5 4d^n 5\ell$ although these array gA values are about an order of magnitude lower than the ones in the 12-14 Å range. Also, the most intense ones are shifted to wavelengths shorter than 10 Å compared to the gold emission.

The major contribution to the continuum in this particular energy range appears to be from ions Bi XXXII to XLV indicating a plasma ionization degree similar to the gold case.

c) uranium spectrum

In the uranium emission (Fig.6c) we observe three intensity steps: the "first" bump rises not very sharply around 10 Å, the second much more clearly at 12.5 Å and the third presents a sharper rise just below 14 Å.

In the spectral region observed, we turn our attention to two basic types of transitions: 4d $\rightarrow$ 5ℓ (ℓ=f,p) and 4f $\rightarrow$ 5ℓ' (ℓ'=g,d). The first group of transitions (4d $\rightarrow$ 5ℓ) from ions U XLVII to U LVI with outer electronic structure $4d^n$ ($10 \geq n \geq 1$) is found to lie at wavelengths shorter than 10 Å; they may correspond to the observed smooth continuum trace with slowly decreasing intensity with wavelength. The 4d-5ℓ satellite transitions in ions with $4d^{10}4f^{n'}$ ($14 \geq n' \geq 1$) outer structure (U XXXIII to U XLVI) are calculated to occur, for 4d-5f, between 14.8 and ~ 10 Å. They could therefore be predominantly associated

with the first bump in the continuum emission while they obviously also contribute to the others. The 4d-5p transitions from the same ion sequence are predicted to extend down to 13.4 Å. They can be associated with the sharp rise of the third bump just below 14 Å.

The second type of transitions ($4f \rightarrow 5\ell'$) in ions with $4f^{n'}$ ground state were calculated to be above 16.5 Å for the 4f-5d arrays and to extend from 21 Å (U XXXIII) to 12.35 Å (U XLVI) for the 4f-5g group. The short wavelength onset of this ion sequence can be associated with the observed second bump on the trace. In Fig.6c, the upper states for the above three transition sequences are indicated.

We note that the ion stages contributing the most to the intensity, appear to be from the 14-ion sequence U XXXIII to U XLVI with much decreased contribution from the high ionization stages.

C) Plasma emission features

In Fig.6 the spectral intensities are in absolute units and may be compared in the gold and in the uranium spectra which were taken under very similar experimental conditions. One observes that, at 10 Å, the thick uranium target radiates a continuum almost four times more intense than the thin gold foil. The intensity produced by the bismuth compound may be read directly from the trace in Fig.5 since the 150 μm-wide slit used with the microfragments was not restricting the illumination. We measured just below 10 Å (that is before the onset of the barium band emission) a radiated intensity of ~ 1.5×10^{17} eV/sr.Å. This corresponds to a radiated energy of ~ 4×10^{10} $W.Å^{-1}.sr^{-1}.cm^{-2}$ assuming that the radiation duration is that of the laser pulse i.e. 4.5 ns and that the plasma surface is 140 μm-wide (laser focal spot diameter) and about 100 μm long.

The observed continuum intensity variations although clearly related, in our experiment, to variations in the laser power and in the laser-heated mass from shot to shot, should also be associated with ionic radiating properties, a consideration of major importance in selecting a suitable target for continuum background emission.

In the three high-Z-element recorded spectra the unresolved N-shell emission contribution appears as an intensity enhancement (bump) on the intense continuum background. Therefore, for elements with Z higher than about 80 and ionized about 40 times or more, the 14-ion sequence with 4f subshell electrons supply a multitude of ion stages and atomic levels responsible for broad band continuous emission. A much larger oscillator strength is also associated with transitions from the 4f level. By correlating the predicted N-shell emission range with intensity steps in the continuum, we also concluded that the three plasmas generated from elements with Z varying over a limited range are of comparable ionization degrees.

The continuum intensity presents a linear slope (in a semi-log plot with an energy scale) that yields a plasma temperature in the region emitting primarily continuum. We derived fairly constant values, in the 200-300 eV range, for the three plasma temperatures.

CONCLUSIONS

The use of high-Z elements as target constituents has proven successful for the generation of soft x-ray continuum of usable intensity by high-power-laser irradiation .

In the intermediate-Z range ($40 < Z < 70$) the 3d-4f unresolved cransition arrays in a 10-ion sequence build up a series of bands or pseudo-continua useful for the observation of absorption edges in solid material (thin foils). Their contribution dominates the spectrum. When the target is constituted of a compound with high-Z elements these bands appear superimposed on the continuum background. Such band systems would prove appropriate for absorption studies if the radiating ion atomic number is matched with the absorption edge energy.

With high-Z materials ($Z \geq 78$), the multitude of 4d-5ℓ transition arrays from a much larger number of available ions appears superimposed on a smooth continuum of very useful intensity in particular above 10 Å. The high intensity continuum corresponds to bremsstrahlung or recombination radiation emission from the denser plasma. Using a bismuth microtarget, we recorded in the 13 Å range, continuum intensities of the order of 5×10^{17} eV/sr-Å. Assuming that the radiation duration is of the order of the laser pulse half width (4.5 ns) and taking for the plasma emitting surface an area about 140 μm wide (focal spot diameter) and 100μm long we can convert the radiated energy to $\sim 1.3 \times 10^{11}$ $W.Å^{-1}.sr^{-1}.cm^{-2}$. Variations in this value by orders of magnitude are to be expected depending on the target size and the laser power density.

This work has focused on microsize targets 140-200 μm in dimension to conserve good spectral resolution when using crystal optics, a feature necessary for discrete absorption studies.

ACKNOWLEDGMENTS

This work was supported by the Defense Nuclear Agency. We acknowledge valuable discussions with R. Elton and H. Griem during the course of this experiment. We appreciate the support of R. Cowan of L.A.N.L. in providing us with his atomic structure code.

REFERENCES

(1) N.R. Pereira and J.Davis, J. Appl. Phys. 64, R2 (1988).

(2) P.K. Carroll, E.T. Kennedy and G.O. Sullivan, Appl. Opt. 19, 1454 (1980).

(3) W. Lampart, R. Weber and J.E. Balmer, J. Appl. Phys. 63, 273 (1988).

(4) P.G. Burkhalter, D.J. Nagel and R.R. Whitlock, Phys. Rev. A 9, 2331 (1974).

(5) P. Mandelbaum, M. Klapisch, A. Bar-Shalom, J.L. Schwob and A. Zigler, Physica Scripta 27, 39 (1983).

(6) N. Tragin, J.P. Geindre, P. Monier, J.C. Gauthier, C. Chenais-Popovics J.F. Wyart and C. Bauche-Arnoult, Physica Scripta 37, 82 (1987).

(7) M. Finkenthal, L.K. Huang, S. Lippmann, H.W. Moos, P. Mandelbaum, J.L. Schwob and M. Klapisch, Phys. Rev. A 127, 255 (1988).

(8) P. Mandelbaum, M. Finkenthal, J.L. Schwob and M. Klapisch, Phys. Rev. A 35, 5051 (1987).

(9) C. Bauche-Arnoult, J. Bauche, and M. Klapisch, Phys. Rev. A 20, 2424 (1979).

(10) P.G. Burkhalter, L. Cohen, R.D. Cowan and B.V. Sweeney, J. Opt. Soc. Am. 72, 95 (1982).

(11) P.G. Burkhalter, U. Feldman and R.D. Cowan, J. Opt. Soc. Am. 64, 1058 (1974).

(12) A. Zigler, M. Givon, E. Yarkoni, M. Kishinevsky, E. Goldberg, B. Arad and M. Klapisch, Phys. Rev. A 35, 280 (1987).

(13) M. Busquet, D. Pain, J. Bauche and E. Luc-Koenig, Physica Scripta 31, 137 (1985).

(14) B.L. Henke, P. Lee, T.J. Tanaka, R.L. Shimabukuro, and B.K. Fujikawa, Atomic Data and Nuclear Data Tables 27, p. 138 Academic, New York (1982).

(15) P.D. Rockett, C.R. Bird, C.J. Hailey, D. Sullivan, D.B. Brown, and P.G. Burkhalter, Appl. Optics 24, 2536 (1985).

(16) D.B. Brown and M. Fatemi, J. Appl. Phys. 51, 2540 (1980).

(17) J.W. Criss, Appl. Spectrosc. 33, 19 (1979).

(18) R.D. Cowan, J. Opt. Soc. Am. 58, 808 (1968).